

# bradscholars

## Structure and blood compatibility of highly oriented poly(l-lactic acid) chain extended by ethylene glycol diglycidyl ether

Item Type	Article
Authors	Li, Z.;Zhao, X.;Ye, L.;Coates, Philip D.;Caton-Rose, Philip D.;Martyn, Michael T.
Citation	Li Z, Zhao X, Ye L et al (2015) Structure and blood compatibility of highly oriented poly(l-lactic acid) chain extended by ethylene glycol diglycidyl ether. Polymer. 56: 523-534.
DOI	<a href="https://doi.org/10.1016/j.polymer.2014.11.035">https://doi.org/10.1016/j.polymer.2014.11.035</a>
Rights	© 2015 Elsevier Ltd. Full-text reproduced in accordance with the publisher's self-archiving policy. This manuscript version is made available under the CC-BY-NC-ND 4.0 license ( <a href="https://creativecommons.org/licenses/by-nc-nd/4.0/">https://creativecommons.org/licenses/by-nc-nd/4.0/</a> )
Download date	2026-03-08 23:42:15
Link to Item	<a href="http://hdl.handle.net/10454/8040">http://hdl.handle.net/10454/8040</a>

# The University of Bradford Institutional Repository

<http://bradscholars.brad.ac.uk>

This work is made available online in accordance with publisher policies. Please refer to the repository record for this item and our Policy Document available from the repository home page for further information.

To see the final version of this work please visit the publisher's website. Available access to the published online version may require a subscription.

**Link to publisher's version:** <http://dx.doi.org/10.1016/j.polymer.2014.11.035>

**Citation:** Li Z, Zhao X, Ye L, Coates PD, Caton-Rose F and Martyn MT (2015) Structure and blood compatibility of highly oriented poly(l-lactic acid) chain extended by ethylene glycol diglycidyl ether. *Polymer*. 56: 523-534.

**Copyright statement:** © 2015 Elsevier Ltd. Full-text reproduced in accordance with the publisher's self-archiving policy.

This manuscript version is made available under the CC-BY-NC-ND 4.0 license  
<http://creativecommons.org/licenses/by-nc-nd/4.0/>.



# **Structure and Blood Compatibility of Highly Oriented Poly(L-lactic acid) Chain Extended by Ethylene Glycol Diglycidyl Ether**

Zhengqiu Li<sup>1</sup>, Xiaowen Zhao<sup>1,\*</sup>, Lin Ye<sup>1</sup>, Phil Coates<sup>2</sup>, Fin Caton-Rose<sup>2</sup>, Michael Martyn<sup>2</sup>

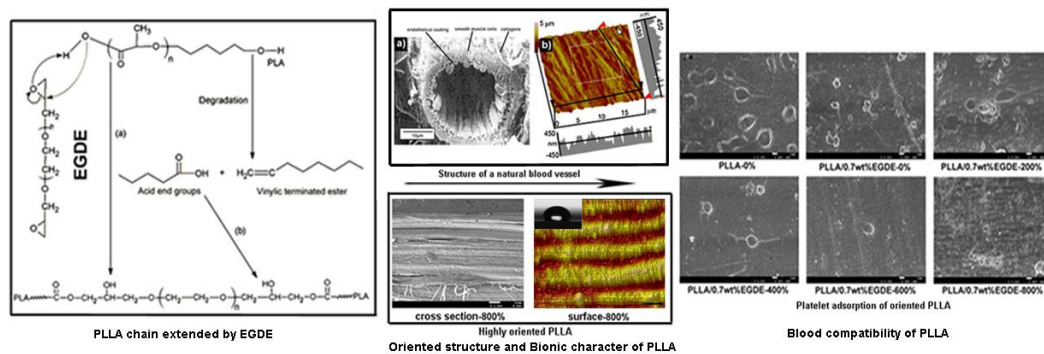
1. State Key Laboratory of Polymer Materials Engineering of China, Polymer Research Institute of Sichuan University, Chengdu, China

2. School of Engineering, Design and Technology, University of Bradford, Bradford, U.K.

\*Corresponding author. Tel.: 862885408802; Fax: 862885402465. E-mail address:

[zhaoxiaowen.scu@126.com](mailto:zhaoxiaowen.scu@126.com)

**Abstract:** Highly-oriented poly(L-lactic acid) (PLLA) were fabricated through chain extension with ethylene glycol diglycidyl ether (EGDE) and solid hot drawing technology. The extending degree as high as 25.79 mol% can be obtained at 0.7wt% EGDE content. The complex viscosity, storage and viscous modulus for chain extended PLLA were improved resulting from the enhancement of molecular entanglement, and consequently higher draw ratio can be achieved during hot stretching. The tensile strength and modulus of PLLA were improved dramatically by stretching. The stress-induced crystallization of PLLA occurred during drawing. The  $\gamma_{s,\text{blood}}$  decreased by chain extension and molecular orientation, indicating the weakened interaction between bioactive substance in the blood and the surface of PLLA. Modification and orientation could significantly enhance the blood compatibility of PLLA by prolonging clotting time and decreasing hemolysis ratio, protein adsorption and platelet activation. The bionic character of oriented PLLA and its anti-coagulation mechanism were tried to be explored.



**Keywords:** Poly (L-lactic acid) (PLLA); chain extension; orientation; mechanical properties; blood compatibility

## **1. Introduction**

Intense effort has been being made on preparing biomedical materials through centuries because of their extensive and significant importance in biology and medicine science [1]. Poly(L-lactic acid) (PLLA) has been considered to be a good candidate for biomedical materials due to its favorable physical properties, ease of handling and processing, and its biodegradable and biocompatible nature, which have been approved by the Food and Drug Administration (FDA) for numerous clinical applications, such as sutures, bone plates, abdominal mesh, and extended-release pharmaceuticals [2~4].

For biomedical materials, two fundamental requirements are proposed. First, their physical properties such as flexibility or rigidity, mechanical strength, etc., must fulfill the purposes for multiple practices relating with biological preference. In addition, for a biomedical implant material to be in contact with blood, the blood compatibility is another one of the most important properties in order to ensure the security of clinical practice [5]. Although extensive efforts have been devoted to modifying the mechanical properties of PLLA by copolymerization with other monomers or chain blending PLLA with other polymers, limited studies have been reported on the blood compatibility of PLLA [6~8].

Solid hot drawing technology presents the advantages of high production rates, high orientation, and significant enhancements in the properties without complex processing apparatus [9~10]. Through solid hot drawing technology, first of all, PLLA with sufficient initial strength and sufficient strength retention over a period of time could be prepared to meet the requirement of desirable physical properties for biomedical use. Meanwhile, the surface properties of PLLA were influenced by processing and thus affect the interaction with the biological elements of the organism. And in our previous work, through solid hot drawing technology, highly oriented PLLA/MWNTs composites and PLLA/TPU blends were prepared

successfully and the most interesting finding was the fact that the oriented samples showed obviously enhanced in vitro blood compatibility as well as mechanical properties [11~12].

However, for neat PLLA, it's very difficult to be ultra-drawn due to its low viscosity and poor melt strength. To overcome such shortcomings, chain extension is the main reported way by which the molecular weight and entanglement between PLLA molecules can be enhanced. Chain extenders are usually bifunctional chemicals which can couple the two end groups of polymer, thereby leading to a linear polymer with a relatively higher molecular weight by means of post polymerization reaction carried during compounding, injection molding, or extrusion. Typical chain extenders for polyesters, which contain –OH and –COOH groups, are diisocyanates, bisoxazolines, dianhydrides and bisketeneacetals diepoxides. J. Kylma et al. synthesised a new kind of l-lactic acid polymers with the use of highly effective carboxyl and hydroxyl reactive chain extenders (2,2-bis(2-oxazoline) (BOX) and 1,6-hexamethylene diisocyanate (HMDI)) [13]. The  $\overline{M}_w$  values of the new polymers were high for realizing good mechanical properties in PLA derivatives. Jukka Tuominen et al. used 2,2'-bis(2-oxazoline) as chain extender for lactic acid based biodegradable polyester, and the effects of polymerization temperature and the amount of 2,2'-bis(2-oxazoline) on the synthesis of lactic acid based poly(ester-amide) were studied [14~15].

Ethylene glycol diglycidyl ether (EGDE) is a bifunctional epoxide compounds which has high reactivity with amines, alcohols, phenols, carboxylic acids and thiols [16]. Thus, EGDE can be used to chain extend poly(methacrylic acid), polyester, poly(imidazole) and so on [17]. Moreover, EGDE is safe and non-toxic, and due to its biological safety, EGDE is even used to prepare DNA network gels [18~20].

In this work, PLLA was chain extended by EGDE through reactive processing, and then the chain extended PLLA with high degree of orientation were fabricated through solid hot drawing technology for the purpose of further improving the mechanical properties and blood

biocompatibility of PLLA as blood-contacting medical devices. The structure and properties of the oriented PLLA were studied.

## **2. Experimental Section**

### **2.1 Materials**

PLLA (3052D) used in this study was supplied by NatureWorks LLC., USA. The molecular weight ( $\overline{M}_w$ ) was about  $1 \times 10^5$ . Ethylene glycol diglycidyl ether (EGDE) (AR) was obtained from Energy Chemical Co. Ltd., China.

### **2.2 Preparation of the Oriented PLLA**

#### **Chain extension of PLLA**

Prior to chain extending, the PLLA was dried at 70°C for 5hrs in a vacuum oven. Chain extended PLLA were prepared by sequentially mixing with EGDE at varying contents (0.1wt% , 0.5wt % , 0.7wt%, 1wt%, 3wt%, 5wt% by weight based on PLLA, respectively) in a Haake internal melt mixer (Rheocord 90, Germany) at 170°C. Then, chain extended PLLA were cut into small granules. Dumbbell shaped specimens were molded by micro-injection molding machine at 170°C. Neat PLLA was treated with the same procedure for comparison.

#### **Orientation of PLLA**

The oriented samples of PLLA and chain extended PLLA were prepared by being heated and mechanically drawn. After the desired draw ratio was obtained, the sample was cooled down to room temperature, and then the load was released.

### **2.3 Measurements**

#### **Molecular weight measurement**

The molecular weight distribution and relative molecular weight of PLLA and chain extended PLLA were determined by a 110 HPLC permeation chromatography (GPC, Agilent Co, USA). PLLA specimens were dissolved in tetrahydrofuran (THF) at a concentration of 5

mg/mL and 10 mL of the test solution was injected into a GPC apparatus (Shimadzu Co., Kyoto, Japan) equipped with two GPC columns (Super HM-H (6.0 mm\*15 cm\*2), Tokyo, Japan), a refractive index detector (model RI, Shimadzu Co.) and Class-LC workstation GPC software(Shimadzu Co.). The flow rate of chloroform mobile phase was 0.6 mL/min. Molecular weight values, including molecular weight ( $\overline{M}_w$  and  $\overline{M}_n$ ) and molecular weight distribution ( $\overline{M}_w/\overline{M}_n$ ) for PLLA were measured from the comparison with the calibration line which was made with polystyrene standards (Showa Denko, Tokyo, Japan).

### **Dynamic rheological measurement**

Dynamic rheological measurement was performed on a dynamic stress AR 1500ex rheometer (TA Instruments, USA). The samples were compression molded into the disk of 25 mm in diameter and around 1 mm in thickness. The measurement was run with a 25 mm-diameter parallel plate geometry and a 1.0-mm sample gap. The dynamic viscoelastic properties were determined with frequencies from 0.01 to 100 Hz at 170°C, using 1% strain (selected after strain sweep tests) value determined with a stress sweep to keep within the linear viscoelastic region. Specimens were placed between the preheated plates at the experimental temperature and were allowed to equilibrate before each run.

### **Non-isothermal crystallization analysis**

The non-isothermal crystallization was performed with a Netzsch 204 differential scanning calorimetry (DSC) (Phoenix Co, Germany). The temperature scale of DSC was calibrated with indium. Granulated samples of about 10 mg were heated from ambient temperature to 200°C at a constant rate of 10 K/min under nitrogen atmosphere.  $X_c$  can be calculated with the following equation:

$$X_c = (\Delta H_m / \Delta H_0) * 100\% \quad (1)$$

where  $\Delta H_m$  is the melting enthalpy of the samples and  $\Delta H_0$  is the balance melting enthalpy,

i.e., the melting enthalpy of 100% crystallizing polymer.

### **Two-dimensional wide-angle X-ray diffraction analysis (2D-WAXD)**

Wide-angle X-ray diffraction (WAXD) analysis was conducted at the ambient temperature using a D8 Discover two-dimensional wide angle X-ray diffractometer (2d-WAXD) (Bruker AXS Co, Germany). The sampling time of 2d-WAXD measurements was 180 s using an Eulerian 1/4 cradle HI-STAR (2D-Detector) detector, with a wavelength of 0.154 nm monochromated X-ray obtained from Cu ( $K_{\alpha}$ ) radiation.

### **Mechanical properties**

The mechanical properties of PLLA samples were measured with a 4302 material testing machine (Instron Co, USA) according to ISO527/1-1993 (E). The test speed was 50 mm/min, and the sample length between benchmarks was 25 mm.

### **Dynamic mechanical analysis (DMA)**

Dynamic mechanical analysis of PLLA and chain extended PLLA samples were performed by using a DMA Q-800 (TA Instruments, USA). Samples were analyzed from -100°C to 150°C temperature range at a heating rate of 3°C/min, 1 Hz frequency in DMA multi frequency strain mode. Size of DMA specimen was 14 mm in length.

### **Contact angle measurement**

The hydrophilicity of the oriented PLLA surface was characterized on the basis of contact angle measurement by means of an OCA20 contact angle goniometer (Dataphysics, Germany) equipped with video capture at ambient temperature 25°C. For the static contact angle measurements, a total of 2 $\mu$ L double distilled water and ethylene glycol (AR) was dropped on the air-side surface of the samples at room temperature, and the contact angle was measured after 10 s. At least five measurements were averaged to get a reliable value.

### **Protein adsorption**

Protein adsorption experiments were carried out with bovine serum albumin (BSA) and bovine serum fibrinogen (BFG) solutions under the static condition. Firstly, the samples with an area of 0.4 cm×0.5 cm was immersed in a phosphate buffer solution (PBS), containing BSA or BFG with the concentration of 1 mg/mL, and incubated at 37°C for 1 h; then the samples was rinsed slightly with PBS solution and double distilled water. Then the samples was placed in a washing solution (2% sodium dodecyl sulfate (SDS) and 0.05 M NaOH) at 37°C, and shaken for 2 h to remove the adsorbed protein. The protein concentration in the washing solution was determined by using the Micro BCATM Protein Assay Reagent Kit (PIERCE), and then the adsorbed protein amount was calculated.

### **Platelet adhesion measurement**

To test the platelet adhesion, samples were incubated with the platelet rich plasma (PRP) for 1 h at 37°C under static conditions. After 1 h incubation, the samples were rinsed carefully three times with phosphate-buffered saline (PBS, pH=7.3) buffer. The adherent platelets were fixed using 2.5% glutaraldehyde in PBS for at least 1 h, dehydrated in a graded series (50%, 60%, 70%, 80%, 90%, 95%, and 100%, v/v) of ethanol, and dried under vacuum at -50°C overnight. The samples were then sputter coated with a thin layer of gold and observed using a scanning electron microscopy (JEOL JSM-5900LV).

### **Hemolysis analysis**

Hemolytic activity was assessed by determining hemoglobin release under static conditions using the two phase hemolysis test (according to ASTM F 756-00). Blood testing solution was prepared by using 4 mL fresh blood with an acid citrate dextrose anticoagulant (ACD medium) and was diluted with 5 ml of physiological saline. In the first phase, each sample was incubated in 10 ml neat saline for 30 min at 37°C. Then, diluted fresh blood (0.2 mL) was added and incubation went on for another 60 min in a shaker at the constant temperature of 37°C. Positive and negative controls were produced by adding 0.2 mL of

diluted fresh blood to 10 ml of purified water and saline, respectively. After incubation, samples were centrifuged at 2500 r/min for 5 min. Optical density of the supernatant was measured at 545 nm by a spectrophotometer. The hemolysis ratio was calculated according to Equation (2):

$$Z=100\%*(D_t-D_{nc})/(D_{pc}-D_{nc}) \quad (2)$$

Where Z represented the hemolysis ratio,  $D_t$  represented the absorbance of test samples,  $D_{nc}$  and  $D_{pc}$  represented the negative samples and positive samples, respectively (ASTM F 756-00).

### **Clotting time (APTT and TT)**

Activated partial thromboplastin time (APTT) and thrombin time (TT) were measured by an automated blood coagulation analyzer CA-50 (Sysmex Corporation, Kobe, Japan), and the test method was described as follows: fresh blood was collected using vacuum tubes, containing sodium citrate as an anticoagulant (anticoagulant to blood ratio, 1:9, v/v). The platelet-poor plasma (PPP) was obtained after centrifuging at 4000 rpm for 15 min. Synchronously, the oriented PLLA and chain extended PLLA samples (0.4 cm×0.5 cm, three pieces) were immersed in PBS (0.2 mL, pH = 7.4) for 1 h. Then the PBS was removed and 0.1 mL of fresh PPP was introduced. After incubating at 37°C for 30 min, 50μL of the incubated PPP was added into the test cup, followed by the addition of 50μL of APTT agent (incubated 10 min before use) and incubation at 37°C for 3 min. Thereafter, 50μL of 0.025 M CaCl<sub>2</sub> solution was added, and then the APTT was measured. For the TT test, 50μL of TT agent was added into the test cup (containing 50μL of the incubated PPP) after 10 min incubating, and then the TT was measured. At least three measurements were averaged to get a reliable value, and the results were analyzed by statistical method.

### **Scanning electron microscope (SEM) analysis**

The fractured surface morphology analysis of the samples was performed with JEOL JSM-5900LV scanning electron microscope (SEM, JEOL Co, Japan) with an acceleration voltage of 20 kV. The samples were sputter-coated with gold for 2~3 min.

### **Atomic force microscopy (AFM) analysis**

The AFM observations were performed on a Dimension 3100 Nanoscope IV equipped with Silicon TESP cantilevers (Shimadzu SPM-9600, Japan) in a non-contact (tapping) mode.

## **3. Results and Discussion**

### **3.1 Chain extension of PLLA**

PLLA was chain extended by di-functional epoxides EGDE through reactive processing. Polyester/epoxide reactions have been widely investigated in the past [21~25], which showed that epoxide groups can react both with terminal carboxyl and terminal hydroxyl groups of polyester. However, according to the literature, the reactivity of epoxide with carboxyl group precedes hydroxyl group, and thus crosslinking and gelation can be avoid during reaction between polyester and di-functional epoxides. [26~28] The proposed mechanism of chain extension of PLLA by EGDE was illustrated in Fig. 1, which involved epoxide ring-opening reactions and the creation of covalent bonds via hydroxyl side group formation. Moreover, due to the low thermal stability of PLLA, the reaction system represented a complex set of degradation and chain extension balance.

#### **3.1.1 Molecular weight**

Fig.2 showed the GPC curves of PLLA before and after chain extension. Clearly, the GPC traces for the both PLLA samples showed a single elution peak, while the characteristic peak with lower outflow time for the chain extended PLLA can be observed. The GPC results such as molecular weight ( $\overline{M}_w$  and  $\overline{M}_n$ ) and the polydispersity ( $\overline{M}_w/\overline{M}_n$ ) of PLLA before and after chain extension were shown in Tab.1, which indicated that the average molecular

weight increased obviously and the polydispersity broadened slightly after chain extension. The molecular weight of chain extended sample was not expected to double its original value, suggesting that chain scission (caused by degradation) also occurred besides the chain extension.

### 3.1.2 Molecular entanglement

Dynamic rheological frequency sweeps were used to determine differences in the entanglement structure for neat and modified PLA samples. Fig. 3(a) showed the complex viscosity ( $\eta^*$ ) as a function of frequency. It was found that curves for both neat PLLA and chain extended PLLA exhibited typical Newtonian behavior and shear thinning behavior. However, all chain extended samples exhibited higher complex viscosities than neat PLLA at full frequency range, and the transition of the complex viscosity curves from Newtonian-plateau to shear thinning regime was shifted to lower frequency indicating the enhanced entanglement between PLLA molecules. With increasing EGDE content, the complex viscosities initially increased and then declined above 1wt% of EGDE due to the plasticizing effect of the unreacted EGDE.

The Cross equation [29] can be applied to investigate the effect of chain extension on the rheological parameters of PLLA, which is written as

$$\eta_{(\omega)}^* = \frac{\eta_0}{1 + (\lambda\omega)^n} \quad (3)$$

where  $\eta_0$  is the Newtonian viscosity,  $\lambda$  is a relaxation time whose reciprocal accounts for the onset of shear-thinning region and  $n$  is a shear-thinning index.

By fitting the experimental data into the Cross equation, rheological parameters such as  $\eta_0$ ,  $\lambda$  and  $n$  can be obtained and were listed in Tab.2. It can be seen that  $\eta_0$  and  $\lambda$  initially

increased steadily with the increase in EGDE content from 0.1 to 0.7wt%, however, it later on decreased somewhat with further rise in content of EGDE. After chain extension,  $n$  decreased.

Since the chain extended samples can be considered as a mixture of original and chain extended components, the zero-shear viscosities of samples after chain extension were assumed to follow a logarithmic mixing rule [30]:

$$\eta_{CL} = \eta_L^{1-x} \eta_{CE}^x \quad (4)$$

$$\eta_{CE} = 2^{3.4} \eta_L = 10.6 \eta_L \quad (5)$$

where,  $x$  is extending degree;  $\eta_{CL}$  is the shear viscosity of modified PLLA;  $\eta_L$  is the shear viscosity of PLLA before chain extension;  $\eta_{CE}$  is the shear viscosity of 100% chain extended PLLA.

The extending degree for PLLA chain extended with 0~1wt% EGDE can be easily obtained from the equation (4) ~ (5) and the values were listed in Tab.2. When extender content increased from 0.1wt%EGDE to 1wt%EGDE, the extending degree increased quickly from 0 to 27.50mol%, indicating that increasing EGDE content was favored to chain extending reaction below 1wt% EGDE content. For samples prepared at higher EGDE content of 3wt% and 5wt%, the calculated extending degree declined because the unreacted extender exerted great effect on the complex viscosities of PLLA.

Cole-Cole plots of PLLA samples were shown as Fig.3 (b). The Cole-Cole plots were close to a semicircle for both the neat and chain extended PLLA, however, the radius of the semicircle increased steadily with the increase in EGDE content from 0.1 to 0.7wt%, indicating the enhanced molecular entanglement between PLLA chains.

Chain extension also caused a dramatic increase in storage modulus ( $G'$ ) and viscous modulus ( $G''$ ) for PLLA. As seen in Fig. 3(c) and (d),  $G'$  and  $G''$  of chain extended PLLA were overall higher than that of neat PLLA and the values reached maximum at 0.7% EGDE

content. This was attributable to more entanglements through formation of physical networks at high molecular weights.

It is known that the melt elasticity and viscosity have a direct relationship with the melt strength which is an indication of the resistance for a melt to extension. Accordingly, the observed improvement in viscous and elastic properties for modified PLLA samples encouraged us to perform solid hot drawing processing on them and high draw ratio can be reached by chain extension as shown in Fig.4.

### **3.2 Orientation structure and properties of drawn PLLA**

#### **3.2.1 Orientation and crystallization properties**

DSC measurements were performed in order to evaluate the influence of processing conditions on the crystallization properties of neat PLLA and chain extended PLLA. The DSC thermograms of isotropic and oriented samples were shown in Fig.5, from which the melting temperature ( $T_m$ ), the heat of melting ( $\Delta H_m$ ) and the crystallinity ( $X_c$ ) can be obtained, as listed in Tab.3.

All samples exhibited three distinct peaks corresponding to glass transition at around 60°C, cold crystallization peaks at about 80-110°C, and melting peaks at around 150°C respectively. Compared with the neat PLLA, the cold crystallization peak became larger, while the glass transition and the melting peak moved to high temperature for chain extended PLLA. Low molecular mobility of chain extended PLLA led to low crystallization rate and imperfect crystallinity.

With the increase of draw ratio, the cold crystallization peak became smaller, while the glass transition and the melting peak moved to high temperature for both neat PLLA and chain extended PLLA. As shown in Tab.3, the melting enthalpy and crystallinity of PLLA increased with the draw ratio, indicating of the stress-induced crystallization of PLLA during drawing.

The WAXD patterns of the PLLA before and after drawing were shown in Fig.6. The isotropic sample did not show any Debye-Scherrer diffraction rings due to its low crystallinity and the random arrangement of grains. While for the samples oriented, the (200)/(110) reflection appeared as two strong circular spots on the equator and (203) reflection formed a four-point image. With increasing draw ratio, these arcs became narrower in spread and more prominent, suggesting that the crystal axis was preferentially oriented perpendicular to the draw direction.

One-dimensional X-ray diffraction curve corresponding to the two-dimensional diffraction pattern was shown in Fig.7. There were two diffraction peaks for the oriented PLLA samples at  $2\theta \approx 16.7^\circ$  and  $18.3^\circ$ , which could be assigned to the crystal planes (200)/(110) and (203) of  $\alpha$  or  $\alpha'$  crystal forms of PLLA, respectively. Previous studies had shown that PLLA can form a disordered  $\alpha$  crystalline form ( $\alpha'$ ) whose chain conformation and chain-packing were different as compared to the ordered  $\alpha$  crystal forms [31~32]. Except for the appearance of (200)/(110) and (203) diffraction peaks, the absence of the (010) and (210) diffraction peaks of  $\alpha$  crystal form at  $2\theta \approx 14.5^\circ$  and  $22.2^\circ$  in our samples indicated that the crystal structure of oriented PLLA could be attributed to the  $\alpha'$  crystalline form. Moreover, the diffraction peak position of PLLA after chain extension had no change indicating that modification did not affect the crystal type of PLLA. The intensity of the diffraction peak represented the degree of the order in the material, including crystallization and orientation. There were significant differences in intensity for samples before and after orientation, suggesting that the degree of crystallization and orientation were greatly enhanced by drawing.

The crystallinity of PLLA can be calculated by the peak area of crystal and amorphous region from the corresponding decomposed curves obtained by PeakFit software. Azimuthal scans ( $0-360^\circ$ ) were performed for the characteristic (200/110) (203) reflections of PLLA. The

Fit-2d package was employed to analyze the resultant 2d-WAXD patterns. The orientation parameter ( $f$ ) was calculated using Herman's orientation function:

$$f = \frac{3 \langle \cos^2 \phi \rangle - 1}{2} \quad (6)$$

$$\langle \cos^2 \phi \rangle = \frac{\int_0^{\pi/2} I(\phi) \sin \phi \cos^2 \phi d\phi}{\int_0^{\pi/2} I(\phi) \sin \phi d\phi} \quad (7)$$

where  $I(\phi)$  is the scattering intensity along the angle  $\phi$ . When taking  $\phi = 0$  as the draw direction, the critical values of  $f$  are -0.5 is considered as a perfect perpendicular orientation, 0 as a random orientation and 1 as a perfect parallel orientation, respectively. The calculated data were summarized in Tab.4.

When the grain size is below  $10\mu\text{m}$ , the polycrystal X-ray diffraction peak broaden remarkably. Based on the widen amount of diffraction peak, the grain size can be calculated with the following equation:

$$L_{\text{hkl}} = \frac{k\lambda}{\beta \cos \theta} \quad (8)$$

Where  $L_{\text{hkl}}$  is the grain size of normal direction of (hkl) crystal plane;  $\theta$  is the Bragg angle;  $\beta$  is the widening amount of diffraction peak attributed to the decrease of the grain size;  $\lambda$  is the wave length of entrance X-ray;  $k$  is a constant.

As shown in Tab.4, with the increase of the draw ratio, the crystallinity and oriented factor of PLLA increased, while the grain size of PLLA decreased, indicating that slipping and rupture of the lamellar in the spherulite occurred during the drawing of PLLA and a clear orientation of PLLA molecules formed.

### 3.2.2 Mechanical properties

The mechanical properties of isotropic and oriented PLLA after chain extension in comparison with neat PLLA were shown in Fig.8. Before orientation, compared to the neat PLLA, chain extension did not bring about remarkable change in tensile strength and

modulus. With increasing drawing ratio, the tensile strength and modulus increased sharply. At 800% of drawing ratio, the tensile strength of the chain extended PLLA can reach up to 101 MPa, and the tensile modulus was 3.9GPa.

Fig.9. showed the temperature dispersions of the dynamic storage modulus and  $\tan \delta$ , and the numerical DMA data of PLLA were listed in Tab.5. The storage modulus increased with draw ratio for both neat PLLA and chain extended PLLA, and the most striking feature was that the very high modulus of 8GPa at  $-100^{\circ}\text{C}$  was achieved for modified PLLA at the draw ratio of 800%. The  $\alpha$  relaxation peak corresponding to the glass transition temperature of PLLA ( $T_g$ ) moved to high temperatures with draw ratio, while the intensity of the peak decreased, which indicated that the local motions of molecular chains in the noncrystalline region and defect region within the crystal were suppressed. Moreover, after chain extension, the  $\tan \delta_{\max}$  increased obviously indicated that the molecular interaction was enhanced.

### 3.2.3 Surface properties

Surface properties such as availability of certain functional groups, domain structure, electrical charge, hydrophilicity/hydrophobicity, interfacial adaptability and surface roughness are considered to determine the fate of blood proteins, enzymes and cells interacting with the materials which, in turn, can induce several cascade reactions and activation phenomena [33]. The contact angles of neat and chain extended PLLA with water and ethylene glycol (EG) as determined by the sessile drop method were listed in Tab.6. The water contact angle increased after chain extension and that value further increased with draw ratio, indicating that orientation and chain extension can enhance the hydrophobicity of PLLA. The EG contact angle also increased with increasing of draw ratio for both PLLA and modified PLLA. The above result indicated that the surface properties of PLLA were significantly influenced by the chain extension reaction and the alignment of PLLA. Therefore, for oriented neat and chain extended PLLA, it was thought that the different blood compatibility may be due to

their different surface properties.

The surface tension and interface tension were determined by contact angle measurements. For a solid-liquid system, the contact angle is related to the surface tension of the liquid and solid by equation (9):

$$\frac{\gamma_{lv}(1 + \cos\theta)}{2\sqrt{\gamma_{lv}^d}} = \sqrt{\gamma_s^d} + \sqrt{\gamma_s^p} \times \sqrt{\frac{\gamma_{lv}^p}{\gamma_{lv}^d}} \quad (9)$$

where  $\theta$  is the contact angle,  $\gamma_s^d, \gamma_s^p$  are the dispersion and polar surface tension of the solid,  $\gamma_{lv}^d, \gamma_{lv}^p$  are the dispersion and polar surface tension of the liquid, and  $\gamma_{lv}$  is the solid/liquid interfacial tension ( $\gamma_{lv} = \gamma_{lv}^d + \gamma_{lv}^p$ ). According to Ref. [34], the values of  $\gamma_{water}^d$ ,  $\gamma_{water}^p$  and  $\gamma_{water}$  are 21.8, 51.0 and 72.8 mN/m respectively; the values of  $\gamma_{EG}^d$ ,  $\gamma_{EG}^p$  and  $\gamma_{EG}$  are 30.9, 16.8 and 47.7 mN/m respectively. After performing a linear fitting, the values of the dispersion tension and polar tension of the solid can be obtained from the slope and intercept, as shown in Tab.6.

Using the  $\gamma_s^d$  and  $\gamma_s^p$  values shown in Tab.6, the interfacial tension  $\gamma_{s,blood}$  between the PLLA surface and blood can be calculated with the following equation and the results were shown in Tab.6.

$$\gamma_{s,blood} = \left\{ \left( \gamma_{blood}^p \right)^{1/2} - \left( \gamma_s^p \right)^{1/2} \right\}^2 + \left\{ \left( \gamma_{blood}^d \right)^{1/2} - \left( \gamma_s^d \right)^{1/2} \right\}^2 \quad (10)$$

where  $\gamma_{blood}^d$  and  $\gamma_{blood}^p$  are the dispersion and polar surface tension of the blood, respectively. According to Ref. [35], the values of  $\gamma_{blood}^p$  and  $\gamma_{blood}$  are 11.2, 36.3 and 47.5 mN/m respectively. From Tab.6, the  $\gamma_{s,blood}$  values decreased as the draw ratio increased while it also decreased by chain extension, indicating that the interaction between bioactive

substance in blood and the surface of PLLA was weakened by modification and orientation. When blood contacts with surface possessing high  $\gamma_{s,\text{blood}}$ , the adsorbed fibrinogen could be anchored onto the solid surface and adheres strongly to the solid surface in order to decrease the solid-liquid interfacial tension. Therefore, the adsorbed proteins could be denatured considerably, and furthermore more fibrinogen could be adsorbed on the surface. On the contrary, for surface with low  $\gamma_{s,\text{blood}}$ , the adsorbed protein would undergo less distortion from its native configuration and less fibrinogen can be adsorbed on surface of it.

### **3.3 Blood compatibility of oriented PLLA**

#### **3.3.1 Protein adsorption**

Protein adsorption on the material surface is a common phenomenon during thrombogenesis. The amount of protein adsorbed on the specimens is reported to be one of the most important factors in evaluating the blood compatibility of materials because protein adsorption is the first event in blood-material interactions [36]. Tab.7. showed the amounts of BSA (bovine serum albumin) and BFG (bovine serum fibrinogen) adsorbed on the neat and chain extended PLLA surfaces from the respective PBS solutions (1 mg/ml). It can be seen that the chain extended PLLA had lower BSA and BFG adsorption than those of the neat PLLA, and the amounts of the adsorbed BSA and BFG decreased further with the increase draw ratios.

#### **3.3.2 Platelet adhesion**

When platelets are activated, they will deform and crosslink to promote aggregation of further platelets. Platelet adhesion and activation on the surface of a biomaterial is the most essential character in determining the blood compatibility of a biomaterial. Low platelet adhesion and activation denotes good blood compatibility, while a higher degree of platelet adhesion and activation could result in a thrombus.

The platelet adhesion densities on the samples were evaluated, as shown in Fig.10. After contact with PRP for 60 min, a large number of platelets were observed to aggregate on the surface of isotropic PLLA. In the case of chain extended PLLA, however, the surface seemed prone to prevent platelets from adhering, since much fewer platelets were observed, indicating that the activation of platelets on chain extended PLLA was limited. Moreover, the platelet adherent density on the modified PLLA after orientation with different draw ratio was significantly lower than that on samples before drawing. In addition, platelets on oriented samples remained the inactivated round shape indicating that activation of the intrinsic blood coagulation system was suppressed.

### **3.3.3 Hemolysis ratio**

Hemolysis of the blood is an extremely serious problem associated with the bio-incompatibility of materials faced by biomaterial researchers. Red blood cells may hemolyze when contacting with implant materials and thus cause eventually failure [37]. Therefore, in evaluating blood compatibility and biocompatibility, it is of vital importance to investigate the hemolysis ratio of the material.

Results obtained from hemolysis test of ACD blood for PLLA and chain extended PLLA were shown in Tab.8. According to the related standard (ASTM F 756-00), permissible hemolysis ratio of biomaterials should be at least lower than 5%. Therefore, first, the hemolysis ratio of 2.03% for neat PLLA makes it suitable as the substrate material. As to the surface of chain extended PLLA before drawing, an obviously less hemolysis rate was obtained indicating that the chain extension would improve the compatibility of the PLLA when contacting with biofluids. Sample after drawing with different draw ratio was much less hemolytic than the isotropic one. Therefore, leading to less damage of red blood cells, the oriented neat and chain extended PLLA exhibited desirable blood compatibility.

### **3.3.4 Clotting time (APTT and TT)**

The APTT (activated partial thromboplastin time) and TT (thrombin time) tests are widely used for the clinical detection of the abnormality of blood plasma and for the primary screening of the anticoagulative chemicals and they are recently applied in the evaluation of the in vitro antithrombogenicity of biomaterials. Tab.9 showed the clotting time of neat PLLA and chain extended PLLA, and all the results were analyzed by statistical methods. It was found that, compared with the neat PLLA before drawing, the APTTs of the chain extended PLLA were longer, and the values increased further with the increase of draw ratio. The enhancement in anticoagulant activity might be resulted from the partial contributions of the increased surface hydrophobicity, decreased protein adsorption, and suppressed platelet adhesion [38~39]. However, the values of TT increased more slowly after chain extension and stretching compared with the APTT. The length of APTT reflects the level of prothrombin, fibrinogen and blood coagulation factors (V and X) in plasma in endogenous pathway of coagulation. TT is mainly affected by the contents of fibrinogen and fibrin in plasma and coagulation activity. The length of TT reflects the level of common path way of coagulation. Therefore, the results indicated that the chain extended PLLA had obvious effect on endogenous pathway of coagulation, which might be attributed to the reaction or combination between the coagulation factors (V and X) in plasma and the hydrophobic surfaces.

### **3.4 Bionic character of oriented PLLA**

The section morphology of chain extended PLLA drawn at different draw ratios were shown in Fig. 11(a-e). It can be seen that the sections of all samples with different draw ratios exhibited orderly arranged fibrillar bundle structure. The sample with the draw ratio of 200% showed larger size and scattered fibrillar bundle whose fibrous structure was the least evident. The sample with the draw ratio of 800% showed concave fibrous structure with regular arranged fibrillar bundle whose fibrous structure was the most evident. These micro-fibers were mainly composed of highly oriented folded lamellar crystals and noncrystal parts

oriented along the drawing direction which alternately and periodically arranged. The formation of these high oriented micro-fibers contributed to the significantly high tensile strength and modulus of the sample.

The surface morphology of PLLA at different draw ratios was shown in Fig. 11(f-j). Surfaces with submicrometer structures, for example alternating parallel grooves and ridges at the micron scale from  $0.60\mu\text{m}$  to  $1.20\mu\text{m}$ , can be observed for the oriented samples. The surface architecture of oriented PLLA was further observed by AFM as shown in Fig.12. With the increase of draw ratio, the depth and width of the grooves both increased. When the draw ratio reached to 800%, the average width of the ridges was about 500nm and the height was about 100 nm.

From the material science point of view, a native blood vessel is the best blood compatible material. The intimal layer of blood vessel can resist platelet adhesion and prevent undesirable thrombus formation [40]. SEM images showed that the inner surface of the aortic intima was not flat but rather rough at the scale of several microns, with fibrillar structure and micro-grooves as shown in Fig.13. This micro topography of the blood vessel was believed to play an important role in blood compatibility because this kind of structure leading to hydrophobicity of surface and a low chance for contact with platelets.

The observed morphology of oriented PLLA was similar to that of the inner surface of blood vessels, and the dimension of these particular surface grooves for oriented PLLA was also closed to that of blood vessels. When the surface roughness was within the range of 50 nm (dimension of proteins) to  $2\mu\text{m}$  (dimension of platelets), particular surface topographies, such as grooves, may reduce the contact area for platelets, which can only adhere on the top of the topographic features; platelet adhesion and thrombus formation may thus be reduced [41].

#### **4. Conclusions**

Highly-oriented PLLA with enhanced melt strength were fabricated through solid hot drawing technology. It was found that extending degree as high as 25.79 mol% can be obtained after chain extension at 0.7wt% EGDE content. The average molecular weight, complex viscosity, storage and viscous modulus as well as molecular entanglement were enhanced by chain extension and higher draw ratio can be achieved. The tensile strength and modulus of samples increased significantly by stretching. The surface properties of PLLA were significantly influenced and the  $\gamma_{s,\text{blood}}$  values decreased by chain extension and molecular orientation, indicating that the interaction between bioactive substance in blood and the surface of PLLA was weakened. The results of in vitro blood compatibility showed that, compared with neat PLLA, oriented samples after chain extension exhibited lower hemolysis ratio, longer clotting time and less platelet and protein adhesion, indicating that the samples with highly molecular orientation exhibited an appreciably better blood compatibility than neat PLLA. Fibrous structure as well as submicrometer structures including alternating parallel grooves and ridges at the micron scale which were similar to intimal layer of blood vessel can be observed for the oriented PLLA, and this structure was considered beneficial to decrease the activation and/or adhesion of platelets.

### **Acknowledgements**

This research was supported by National Natural Science Foundation of China (Grant No. 51303109).

## References

- [1] B.D. Ratner, S.J. Bryant, *Annu Rev Biomed Eng*, 6 (2004), p.41.
- [2] K. [Rezwan](#), Q.Z. [Chen](#), J.J. [Blaker](#), A.R. [Boccaccini](#), *Biomaterials*, 27(2006), p.3413.
- [3] W.Y. [Yeong](#), C.K. [Chua](#), K.F. [Leong](#), M. [Chandrasekaran](#), *Trends in Biotechnol* 22(2004), p.643.
- [4] J.W. [Xie](#), M.R. [MacEwan](#), W.Z. [Ray](#), W. [Liu](#), D.Y. [Siewe](#), Y.N. [Xia](#), *ACS Nano* 4(2010), p.5027.
- [5] W.K. Czaja, D.J. Young, M. Kawecki, R.M. Brown, *Biomacromolecules*, 8(2007), p.1.
- [6] S.L. [Bourke](#), J. [Kohn](#), *Adv Drug Del Rev*, 55(2003), p.447.
- [7] A.K. Gupta, M. Gupta, *Biomaterials*, 26(2005), p.3995.
- [8] P. [Gunatillake](#), R. [Mayadunne](#), R. [Adhikari](#), *Biotechnol Ann Rev*, 12(2006), p.301.
- [9] G. Stoclet, R. Seguela, J.M. Lefebvre, S. Elkoun, C. Vanmansart, *Macromolecules*, 43(2010), p.1488.
- [10] X.W. [Zhao](#), L. [Ye](#), *Compos Sci Technol*, 71(2011), p.1367.
- [11] X.W. Zhao, L. Ye, P. Coates, F.C. Rose, M. Martyn, *Polym Adv Technol*, 24(2013), p.853.
- [12] Z.Q. Li, X.W. Zhao, L. Ye, P. Coates, F.C. Rose, M. Martyn, *J Biomater Appl*  
Published online before print June 2, 2013.
- [13] K. [Hiltunen](#), M. [Härkönen](#), J.V. [Seppälä](#), T. [Väänänen](#), *Macromolecules*, 29(1996), p.8677.
- [14] J. [Kylmä](#), J. [Tuominen](#), A. [Helminen](#), J. [Seppälä](#), *Polymer*, 42(2001), p.3333.

- [15] J. [Tuominen](#), J.V. [Seppälä](#), *Macromolecules*, 33(2000), p.3530.
- [16] C. [Wendeln](#), B.J. [Ravoo](#), *Langmuir*, 28(2012), p.5527.
- [17] M.D. Bentley, X. Zhao, X. Shen, W.D. Battle, US Patent No. 7026440, 2013.
- [18] M.J. Campolongo, S.J. [Tan](#), J. Xu, D. Luo, *Adv Drug Del Rev*, 62(2010), p.606.
- [19] N. Orakdogan, B. Erman, O. Okay, *Macromolecules*, 43(2010), p.1530.
- [20] D. Costa, J. Queiroz, M.G. Miguel, B. Lindman, *Colloid Surf B Biointerfaces*, 92(2012), p.106.
- [21] D.S. Achilias, H.H. Redhwi, M.N. Siddiqui, A.K. Nikolaidis, D.N. Bikiaris, *J Appl Polym Sci*, 118(2010), p.3066.
- [22] A.A. Haralabakopoulos, D. Tsiourvas, C.M. Paleos, *J Appl Polym Sci*, 71(1999), p.2121.
- [23] L. Incarnato, P. Scarfato, L.D. Maio, D. Acierno, [Polymer](#), 41(2000), p.6825.
- [24] S. [Japon](#), L. [Boogh](#), Y. [Leterrier](#), J.A. [Månson](#), [Polymer](#), 41(2000), p.5809.
- [25] C. [Decker](#), T.N. [ThiViet](#), D. [Decker](#), E.W. [Koehl](#), [Polymer](#), 42(2001), p.5531.
- [26] G.K. Toworfe, R.J. Composto, I.M. Shapiro, P. Ducheyne, *Biomaterials*, 27(2006), p.631.
- [27] K. Lamnawar, A. Maazouz, *Rheol acta*, 45(2006), p.411.
- [28] K. Lamnawar, A. Baudouin, A. Maazouz, [Eur Polym J](#), 46(2010), p.1604.
- [29] S.A. [Madbouly](#), J.U. [Otaigbe](#), A.K. [Nanda](#), D.A. [Wicks](#), *Macromolecules* 38(2005), p.4014.
- [30] J. Liu, L. Lou, W. Yu, R. Liao, R. [Li](#), C. Zhou, [Polymer](#), 51(2010), p.5186.

- [31] J. [Zhang](#), Y. Duan, A.J. [Domb](#), Y. Ozaki, *Macromolecules*, 43(2010), p.4240.
- [32] K. Wasanasuk, K. Tashiro, M. Hanesaka, T. Ohhara, *Macromolecules*, 44(2011), p.6441.
- [33] X. Zhang, F. [Shi](#), J. [Niu](#), Y. Jiang, Z. Wang, *J Mater Chem*, 18(2008), p.621.
- [34] Y.X. Zhuang, O. [Hansen](#), *Langmuir*, 25(2009), p.5437.
- [35] S. Agathopoulos, P. Nikolopoulos, *J Biomed Mater Res*, 29(1995), p.421.
- [36] J. Xue, W. [Zhao](#), S. Nie, S. Sun, C. Zhao, *Carbohydr polym*, 95(2013), p.64.
- [37] X.W. Wen, S.P. Pei, H. Li, F. Ai, H. Chen, K.Y. Li, *J Mater Sci*, 45(2010), p.2788.
- [38] H. Liu, J. Zhai, L. Jiang, *Soft Matter*, 2(2006), p.811.
- [39] H. Fan, P. Chen, R. Qi, J. Zhai, D. Han, L. Jiang, *Small*, 19(2009), p.2144.
- [40] A.D. [Mel](#), G. [Jell](#), M.M. [Stevens](#), A.M. [Seifalian](#), *Biomacromolecules*, 9(2008), p.2969.
- [41] L. Chen, D. Han, L. Jiang, *Colloid Surf B Biointerfaces*, 85(2011), p.2.
- [42] D. Klee, H. Hocker, *Adv Polym Sci*, 149(1999), p.1.

**Table caption**

**Tab. 1.** GPC results of PLLA

**Tab. 2.** Rheological parameters of PLLA

**Tab. 3.** DSC parameters of oriented PLLA

**Tab. 4.** Crystallinity, orientation factor and grain size of oriented PLLA

**Tab. 5.** DMA parameters of oriented PLLA

**Tab. 6.** Contact angles and surface tension of oriented PLLA

**Tab. 7.** BSA and BFG adsorptions on the oriented PLLA

**Tab. 8.** Hematolysis ratio of oriented PLLA

**Tab. 9.** Clotting time of oriented PLLA

**Table 1** GPC results of PLLA

Samples	$\overline{M}_n$ ( $\times 10^4$ )	$\overline{M}_w$ ( $\times 10^4$ )	$\overline{M}_w/\overline{M}_n$
PLLA	5.092	10.399	1.850
PLLA/0.7wt%EGDE	6.218	11.805	1.899

**Table 2** Rheological parameters of PLLA

Samples	$\lambda$ (s)	n	$\eta_{0, CL}$ (Pa.s)	Extending degree (mol%)
PLLA	0.049	1.724	868	0
0.1wt%EGDE	0.034	0.963	539	0
0.5wt%EGDE	0.056	0.775	1319	17.75
0.7wt%EGDE	0.061	0.820	1595	25.79
1wt%EGDE	0.062	0.757	1661	27.50

**Table 3** DSC parameters of oriented PLLA

Samples	Draw ratio (%)	$T_m$ ( $^{\circ}$ C)	$\Delta H$ (J/g)	$X_c$ (%)
PLLA-0%	0	151.7	36.18	38.90
PLLA-200%	200	150.6	36.13	38.85
PLLA-400%	400	151.0	40.12	43.14
PLLA-600%	600	150.5	42.06	45.23
PLLA/EGDE-0%	0	152.7	34.49	37.09
PLLA/EGDE-200%	200	151.6	38.57	41.47
PLLA/EGDE-400%	400	150.5	38.51	41.41
PLLA/EGDE-600%	600	149.0	38.56	41.46
PLLA/EGDE-800%	800	148.7	39.31	42.27

**Table 4** Crystallinity, orientation factor and grain size of oriented PLLA

Samples	Orientation Factor	Crystallinity(%)	Grain size(Å)
PLLA-0%	0.00098	30.2	184
PLLA-200%	0.04938	38.9	164
PLLA-400%	0.28606	41.2	92
PLLA-600%	0.29999	44.3	65
PLLA/EGDE-0%	0.00144	30.0	186
PLLA/EGDE-200%	0.10276	35.5	173
PLLA/EGDE-400%	0.26315	39.1	113
PLLA/EGDE-600%	0.29892	42.4	99
PLLA/EGDE-800%	0.31549	46.3	58

**Table 5** DMA parameters of oriented PLLA

Samples	Tan $\delta$	T <sub>g</sub> (°C)
PLLA-0%	2.111	71.53
PLLA-200%	0.5215	78.42
PLLA-400%	0.5226	78.53
PLLA-600%	0.5298	79.23
PLLA/EGDE-0%	2.348	72.39
PLLA/EGDE-200%	0.5513	79.64
PLLA/EGDE-400%	0.4256	80.79
PLLA/EGDE-600%	0.3456	80.45
PLLA/EGDE-800%	0.4386	81.21

**Table 6** Contact angles and surface tension of oriented PLLA

Samples	Contact Angle(°)		$\gamma_s^d$ (mN/m)	$\gamma_s^p$ (mN/m)	$\gamma_s$ (mN/m)	$\gamma_{s.blood}$ (mN/m)
	Water	EG				
PLLA-0%	74.7	48.1	31.50	60.35	51.85	8.17
PLLA-200%	75.5	49.7	31.62	59.37	50.60	8.01
PLLA-400%	77.7	50.9	29.68	58.72	48.39	7.10
PLLA-600%	82.2	54.2	26.75	54.65	41.39	5.20
PLLA/EGDE-0%	83.3	48.3	23.90	32.37	36.27	2.49
PLLA/EGDE-200%	86.6	50.3	22.42	43.88	26.30	2.29
PLLA/EGDE-400%	90.5	51.7	20.98	42.13	23.11	1.74
PLLA/EGDE-600%	97.0	58.2	20.14	41.56	21.70	1.48
PLLA/EGDE-800%	99.2	59.8	20.02	40.86	20.87	1.41

**Table 7** BSA and BFG adsorptions on the oriented PLLA

Samples	BSA( $\mu\text{g}/\text{cm}^2$ )	BFG ( $\mu\text{g}/\text{cm}^2$ )
PLLA-0%	5.623	0.070
PLLA-200%	2.369	0.001
PLLA-400%	1.569	0
PLLA-600%	1.561	0.012
PLLA/EGDE-0%	2.816	0.020
PLLA/EGDE-200%	2.737	0.011
PLLA/EGDE-400%	1.977	0
PLLA/EGDE-600%	2.314	0
PLLA/EGDE-800%	0.396	0

**Table 8** Hematolysis ratio of oriented PLLA

Samples	Hematolysis ratio (%)
PLLA-0%	2.033
PLLA-200%	0.879
PLLA-400%	0.250
PLLA-600%	0
PLLA/EGDE-0%	1.467
PLLA/EGDE-200%	0.973
PLLA/EGDE-400%	0.606
PLLA/EGDE-600%	0
PLLA/EGDE-800%	0

**Table 9** Clotting time of oriented PLLA

Samples	APTT(s)	TT(s)
Plasma	19.2	20.1
PLLA-0%	8.6	20.0
PLLA-200%	9.7	18.9
PLLA-400%	11.9	21.8
PLLA-600%	14.1	22.5
PLLA/EGDE-0%	15.2	19.4
PLLA/EGDE-200%	17.8	20.1
PLLA/EGDE-400%	20.7	21.7
PLLA/EGDE-600%	22.0	22.1
PLLA/EGDE-800%	23.1	23.3

## **Figure caption**

**Fig. 1.** Proposed reaction between PLLA and EGDE

**Fig. 2.** GPC curves of PLLA

**Fig. 3.** (a) Complex viscosity versus frequency for PLLA at 170°C; (b) Cole-Cole plot; (c) Elastic modulus versus frequency for PLLA at 170°C; (d) Viscous modulus versus frequency for PLLA at 170°C.

**Fig. 4.** The maximum draw ratios of PLLA

**Fig. 5.** DSC curves of oriented PLLA

**Fig. 6.** Two-dimensional XRD pattern of oriented PLLA

**Fig. 7.** WAXD curves of oriented PLLA

**Fig. 8.** Mechanical properties of oriented PLLA

**Fig. 9.** Dynamic mechanical properties of PLLA

**Fig. 10.** Platelet adsorption of oriented PLLA (Magnification: 5000×)

**Fig. 11.** SEM images of oriented PLLA: (a-e) cross-sections; (f-j) surfaces.

**Fig. 12.** AFM images of PLLA surfaces. Scale bars: 500 nm

**Fig. 13.** Structure of a natural blood vessel (a) SEM image, adopted from Ref.[41];(b) In vivo AFM imaging of blood vessel tissues of living rats, from which micro-grooves and nano-protuberances can be observed, adopted from Ref.[42].

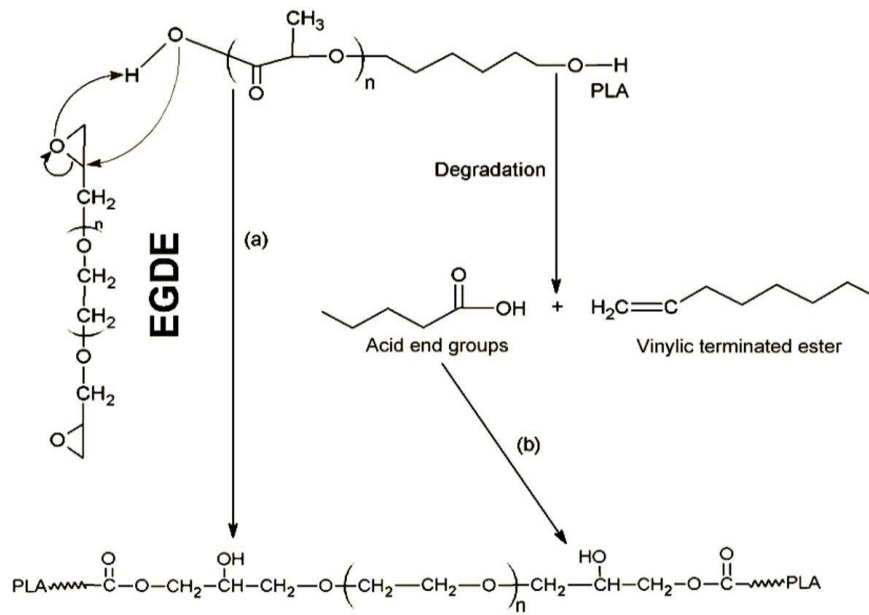


**Figure 1** Posed reaction between PLLA and EGDE

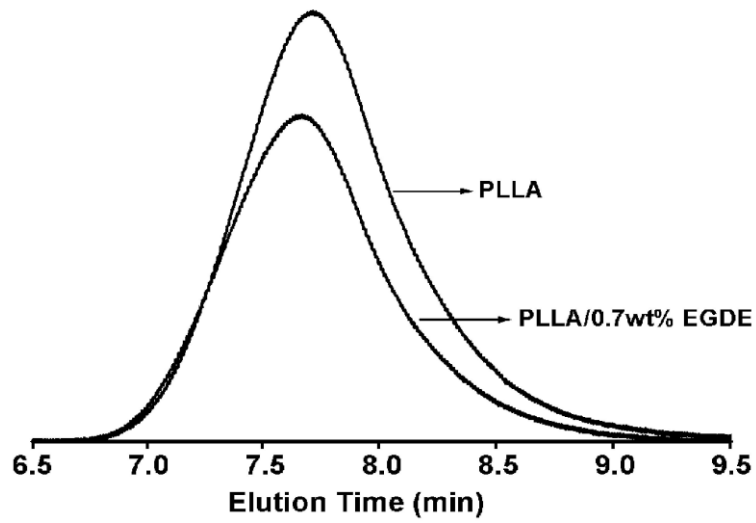


**Figure 2** GPC curves of PLLA

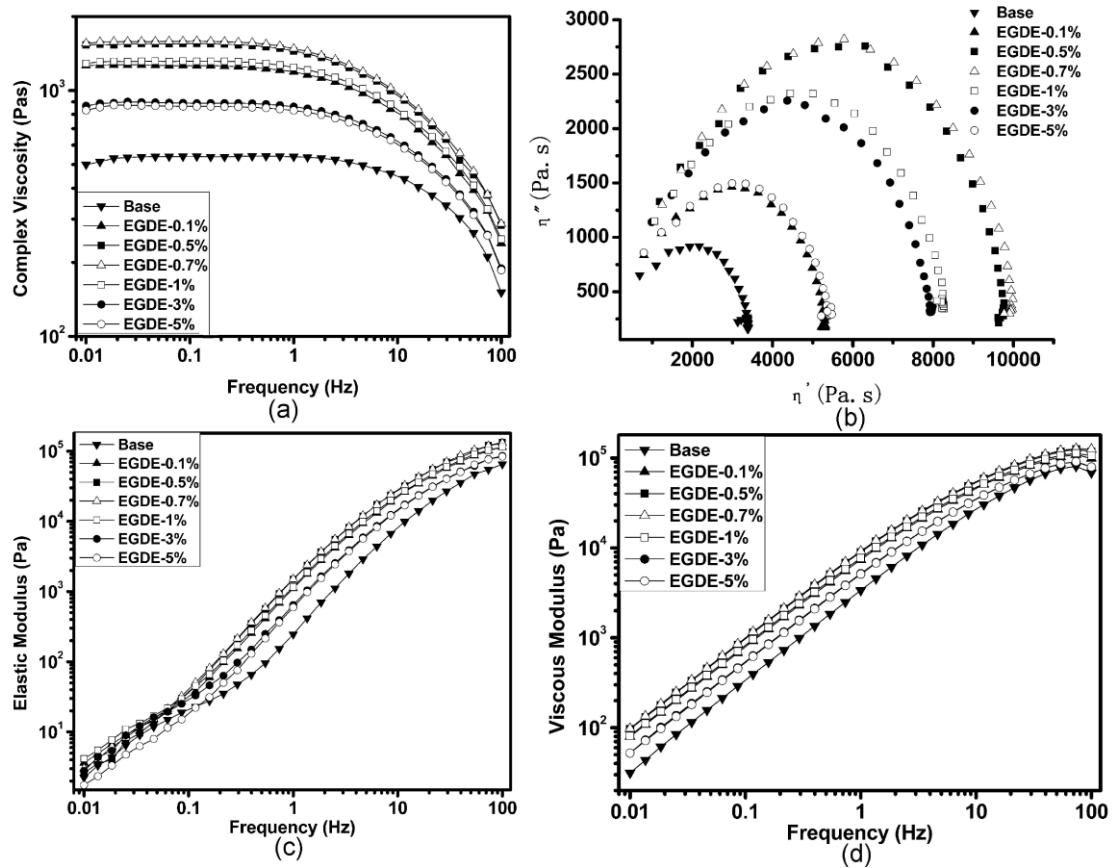


**Figure 3** (a) Complex viscosity versus frequency for PLLA at 170°C; (b) Cole-Cole plot; (c) Elastic modulus versus frequency for PLLA at 170°C; (d) Viscous modulus versus frequency for PLLA at 170°C.

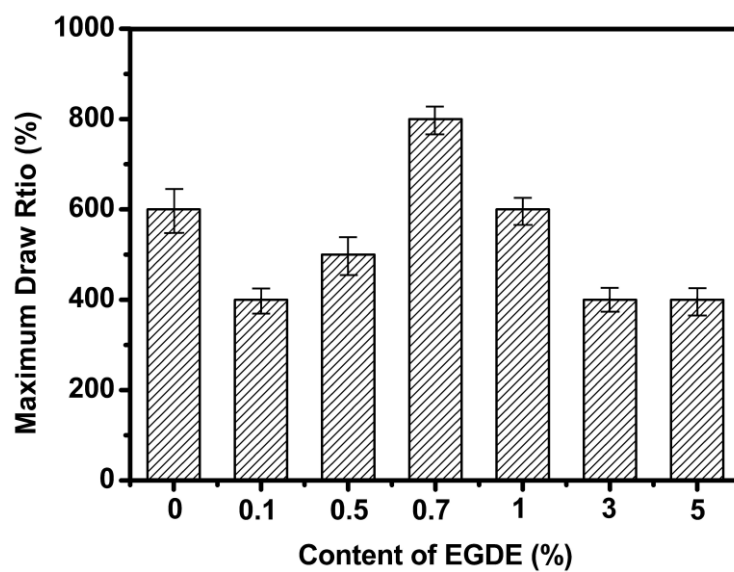


**Figure 4** The maximum draw ratios of PLLA

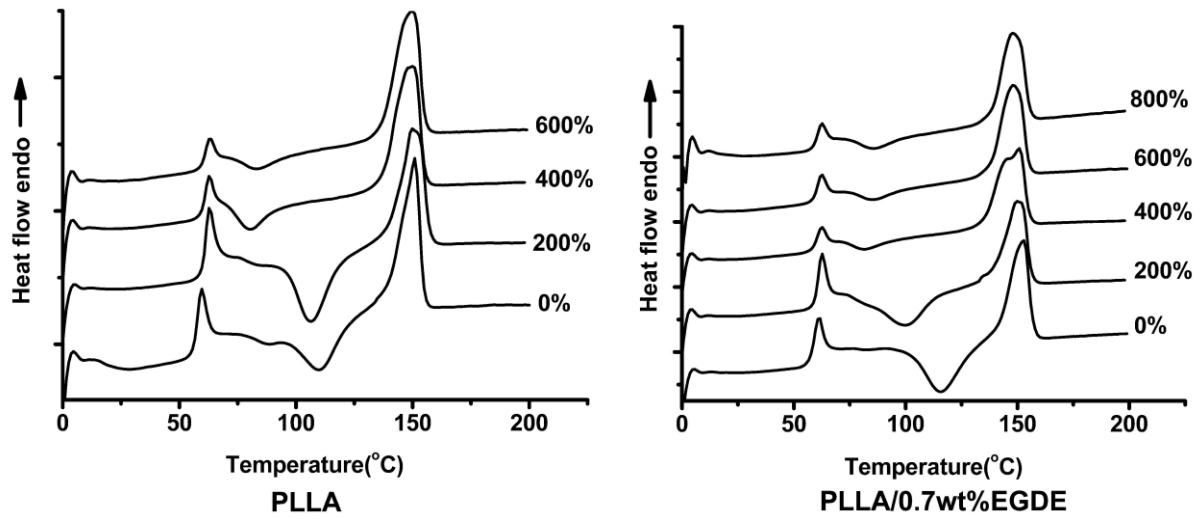


Figure 5 DSC curves of oriented PLLA

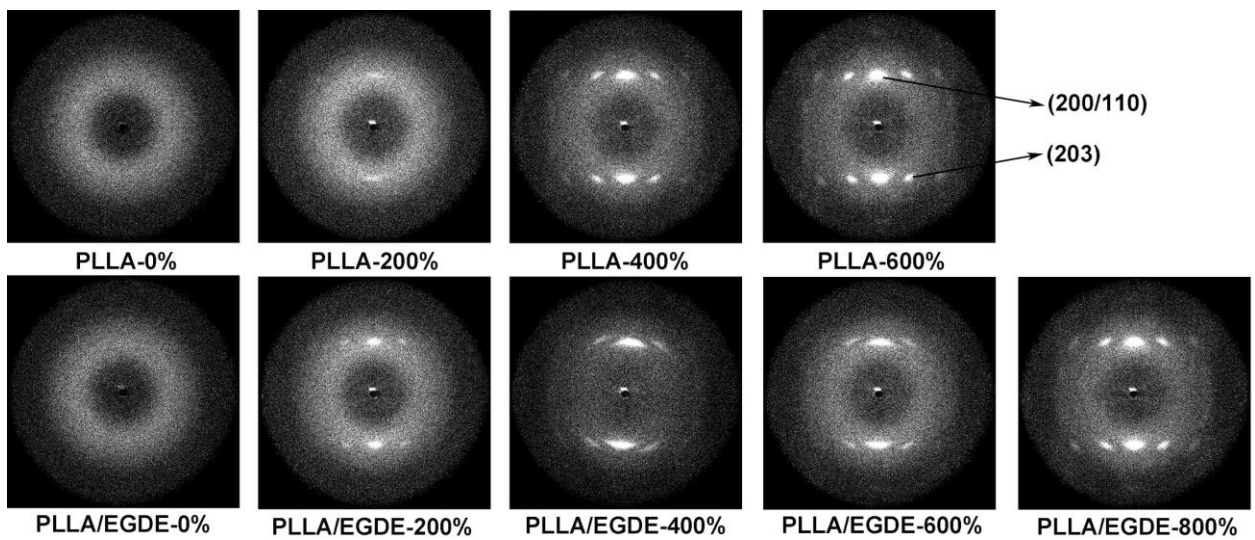


Figure 6 Two-dimensional XRD pattern of oriented PLLA

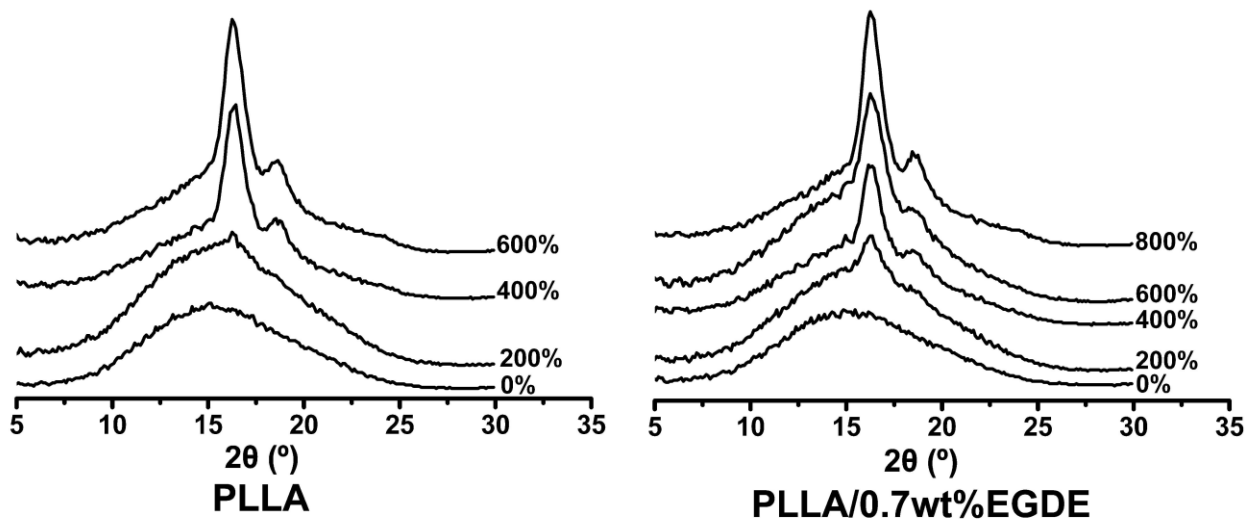


Figure 7 WAXD curves of oriented PLLA

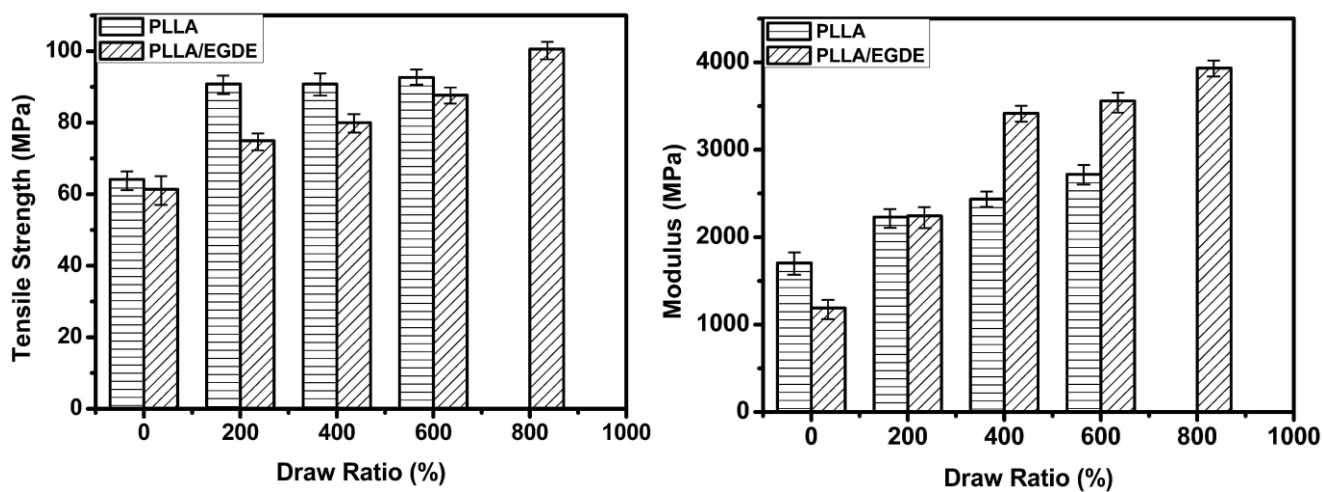


Figure 8 Mechanical properties of oriented PLLA

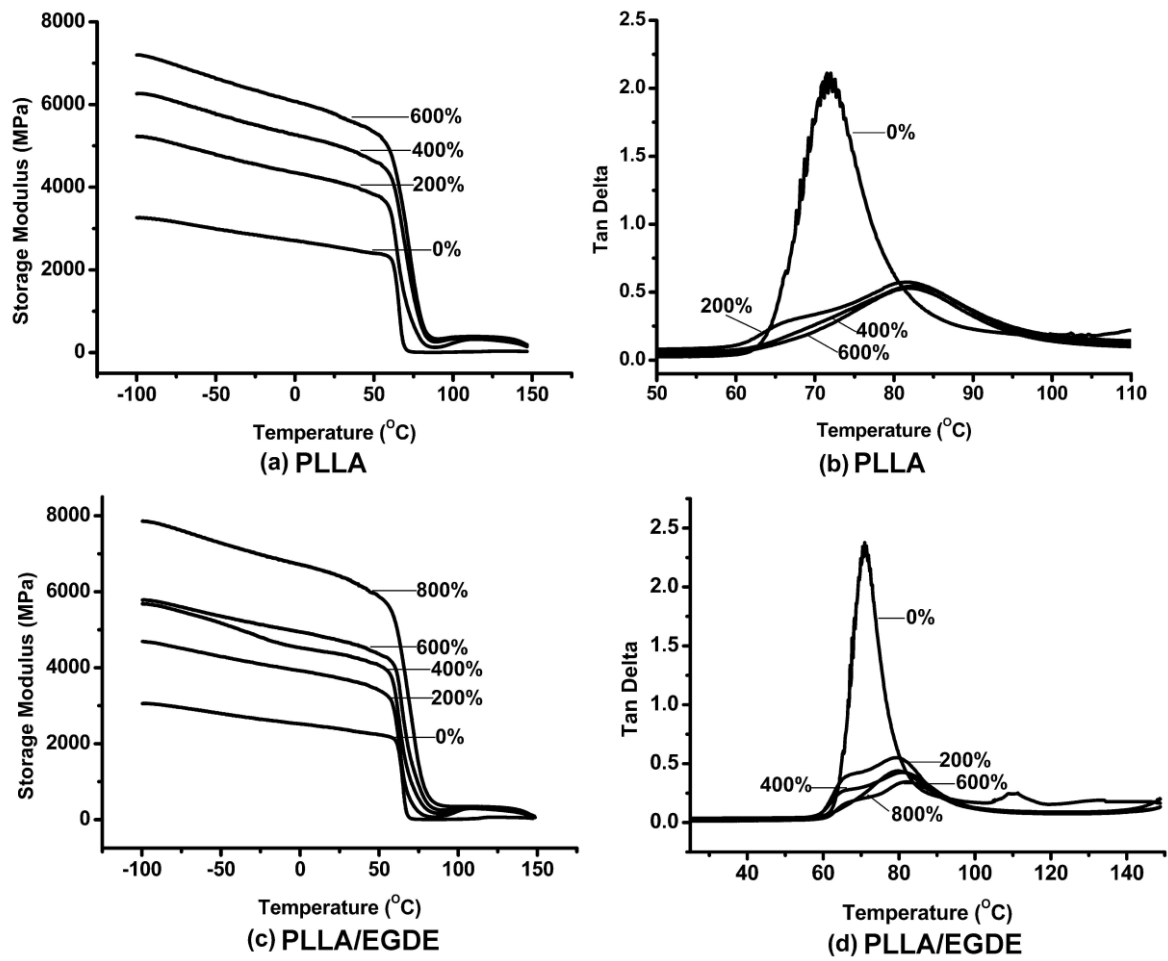


Figure 9 Dynamic mechanical properties of PLLA

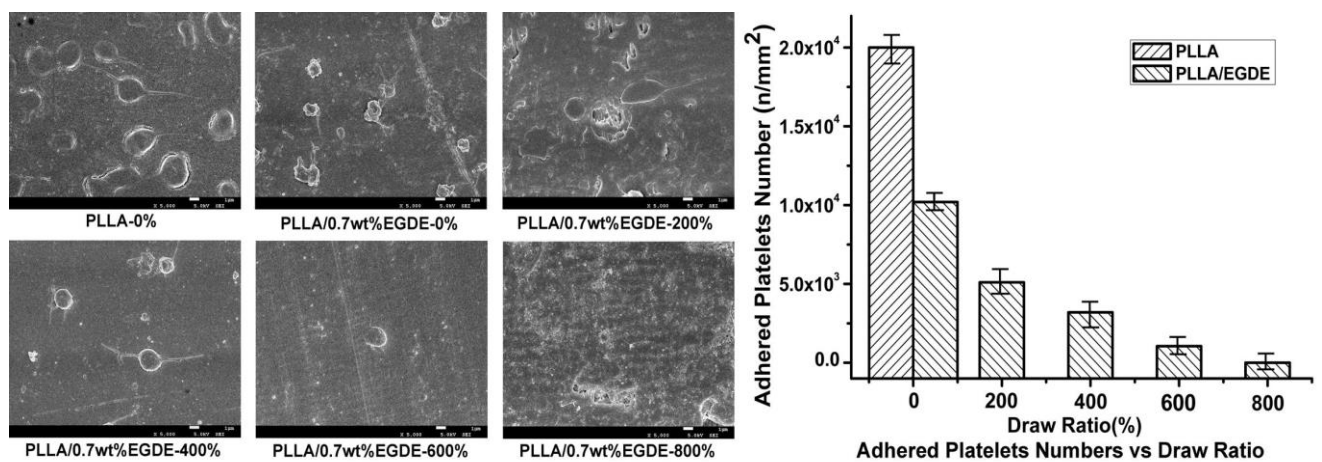
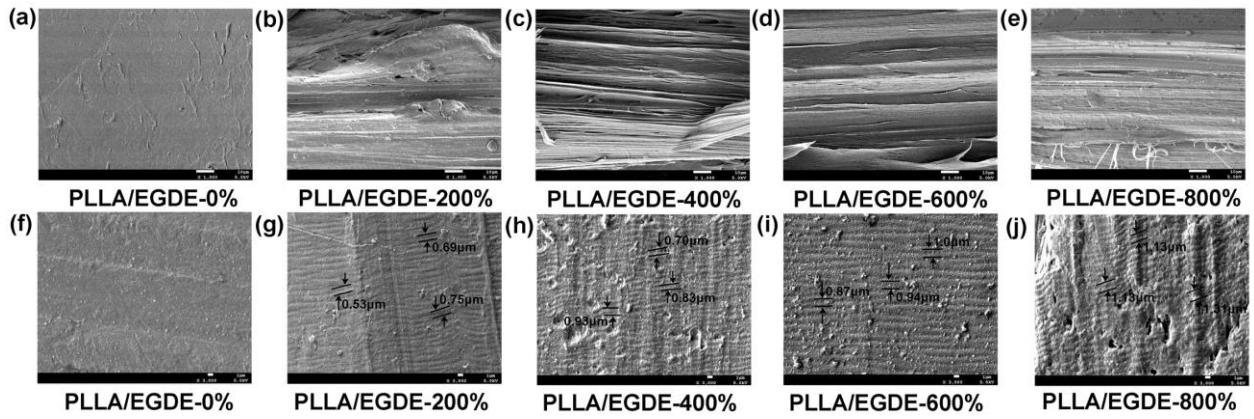
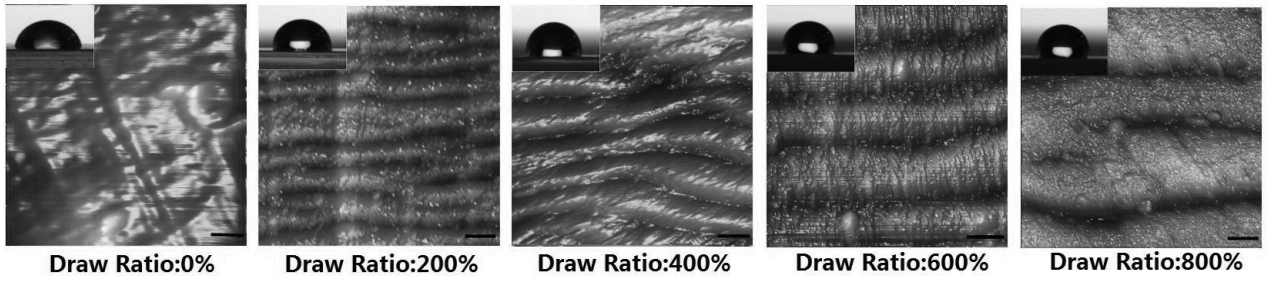


Figure 10 Platelet adsorption of oriented PLLA (Magnification: 5000×)



**Figure 11** SEM images of oriented PLLA: (a-e) cross-sections; (f-j) surfaces



**Figure 12** AFM images of PLLA surfaces. Scale bars: 500 nm

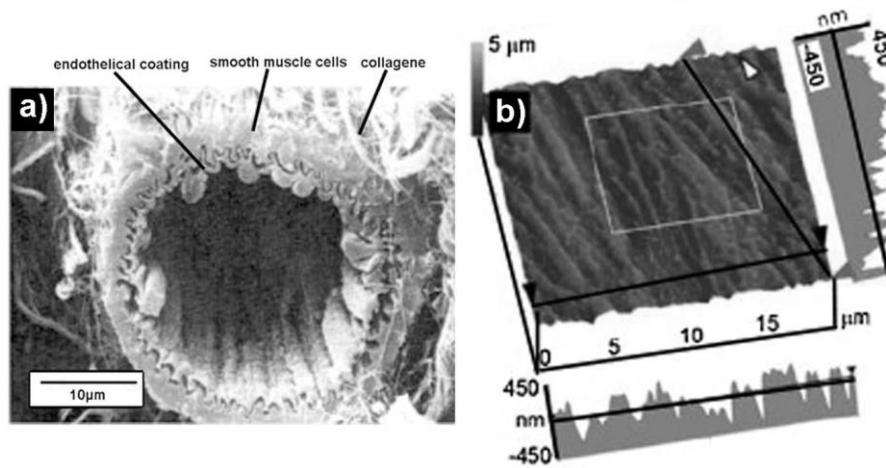


**Figure 13** Structure of a natural blood vessel (a) SEM image, adopted from Ref.[41];(b) In vivo AFM imaging of blood vessel tissues of living rats, from which micro-grooves and nano-protuberances can be observed, adopted from Ref.[42].